Mineralogical Magazine, April 2018, Vol. 82(2), pp. 257–274

Saranchinaite, $Na_2Cu(SO_4)_2$, a new exhalative mineral from Tolbachik volcano, Kamchatka, Russia, and a product of the reversible dehydration of kröhnkite, $Na_2Cu(SO_4)_2(H_2O)_2$

Oleg I. Siidra[1,2,*], Evgeniya A. Lukina[1], Evgeniy V. Nazarchuk[1], Wulf Depmeier[3], Rimma S. Bubnova[1], Atali A. Agakhanov[4], Evgeniya Yu. Avdontseva[1], Stanislav K. Filatov[1] and Vadim M. Kovrugin[1]

[1] Department of Crystallography, St. Petersburg State University, 7–9 University Emb., St. Petersburg 199034, Russia
[2] Nanomaterials Research Center, Kola Science Center, Russian Academy of Sciences, Apatity, Murmansk Region, 184200, Russia
[3] Institut für Geowissenschaften der Universität Kiel, Olshausenstr. 40, Kiel, D-24098, Germany
[4] Fersman Mineralogical Museum, Russian Academy of Science, Leninskii Pr-t, Bldg. 18, Moscow 117071, Russia

[*Received 16 March 2017; Accepted 17 May 2017; Associate Editor: Ed Grew*]

ABSTRACT

The new mineral saranchinaite, ideally $Na_2Cu(SO_4)_2$, was found in sublimates of the Saranchinaitovaya fumarole, Naboko Scoria Cone, Tolbachik volcano, Kamchatka, Russia. Its discovery and study has enabled the characterization of the thermal decomposition of kröhnkite and provided an insight into the high-temperature behaviour of other kröhnkite-type materials. Saranchinaite is monoclinic, $P2_1$, $a = 9.0109(5)$, $b = 15.6355(8)$, $c = 10.1507(5)$ Å, $\beta = 107.079(2)°$, $V = 1367.06(12)$ Å^3, $Z = 8$ and $R_1 = 0.03$. Saranchinaite is a unique mineral in that two of its four independent Cu sites display a very unusual Cu^{2+} coordination environment with two weak Cu–O bonds of ~2.9–3.0 Å, resulting in [4+1+2] CuO_7 polyhedra. Each of the Cu-centred polyhedra shares common corners with SO_4 tetrahedra resulting in a $[Cu_4(SO_4)_8]^{8-}$ framework with a complex channel system occupied by Na atoms. Saranchinaite is sensitive to moisture and transforms into kröhnkite within one week when exposed to open air at 87% relative humidity and 25°C. High-temperature X-ray diffraction studies were performed for both kröhnkite (from La Vendida mine, Antofagasta Region, Chile) and saranchinaite. During thermal expansion kröhnkite retains its strongly anisotropic character up to its full dehydration and the formation of saranchinaite at ~200°C, which then transforms back into kröhnkite after exposure to open air. The thermal expansion of saranchinaite is more complex than that of kröhnkite. Saranchinaite is stable up to 475°C with subsequent decomposition into tenorite CuO, thénardite Na_2SO_4 and unidentified phases.

Keywords: sulfates, hydration, dehydration, high-temperature X-ray diffraction, framework structures, copper coordination, new mineral, saranchinaite, kröhnkite, Tolbachik Fissure eruption 2012–2013.

Introduction

Sulfate-containing minerals constitute a rich family with more than 380 different species known to date. The formation of sulfate minerals in the oxidation zones of sulfide deposits represents an important factor affecting the redox conditions of the environment and the transport of secondary phases. Most known sulfate minerals are hydrated, but a significant number of anhydrous sulfate minerals formed as a result of high-temperature exhalative processes in the fumaroles of some volcanoes e.g. Vesuvius, Italy (Demartin *et al.*, 2012); Tolbachik, Russia (Siidra *et al.*, 2017); and Eldfell, Iceland (Balić-Žunić *et al.*, 2009). Many of these minerals are unstable under ambient terrestrial conditions and the study of their structural and physicochemical properties is challenging.

*E-mail: o.siidra@spbu.ru
https://doi.org/10.1180/minmag.2017.081.037

The volcanogenic exhalation sulfate mineralization from fumaroles of the Tolbachik volcano is renowned for its rich mineral diversity (Vergasova and Filatov, 2016). Despite the large number of previous studies on different minerals discovered in this unique deposit, hydration and weathering processes of the primary volcanogenic mineral assemblages have not been studied in detail. However, it is clear that complex multistage physicochemical processes are involved which require detailed and rather elaborate studies to understand them.

During the past decade or so, the experimental mineralogy of sulfates has attracted considerable attention because remote sensing and direct sampling from satellites and rovers have resulted in the discovery of the various sulfate minerals on Mars (Peterson and Wang, 2006). As most Martian sulfate minerals have been found to be hydrated this observation suggests the existence of liquid water on Mars, at least in its early history (Vaniman *et al*., 2004; Szynkiewicz *et al*., 2014), which opens the possibility that early Mars might have been habitable and life in some form might have existed. This explains in part the ongoing and planned exploration activities with regard to Mars (e.g. Vasavada, 2017). As safe return of unaltered Martian samples to Earth is unlikely to be successful in the near future because of the instability of hydrous sulfates and their easy transformation into different phases, for instance as a result of changing temperatures, laboratory experiments performed on Earth have to simulate current and past conditions on the surface of Mars. Results of recent temperature-dependent X-ray diffraction (XRD) and Raman spectroscopy studies on hydrous and anhydrous sulfate minerals have been reported (e.g. Leftwich *et al*., 2012; Wang and Zhou, 2014; Mills *et al*., 2010, 2013).

Kröhnkite, $Na_2Cu(SO_4)_2(H_2O)_2$ was first described 130 years ago (Domeyko, 1879) from samples found in the famous Chuquicamata Mine in Chile. Kröhnkite crystals up to 5 cm long are known from the oxidized zones of copper deposits in very arid conditions in the Atacama Desert. The structure of kröhnkite was first determined by Dalman (1952) and later refined by Hawthorne and Ferguson (1975). Its thermodynamic properties were studied recently by Majzlan *et al*. (2016) who demonstrated the necessity of having high molality of Cu^{2+}, alkali ions and $(SO_4)^{2-}$ in the aqueous solution for kröhnkite to form. By means of high-temperature (HT) XRD, thermal analysis and emission infrared spectroscopy, Testasicca *et al*. (2016) reported kröhnkite to decompose "into a complex mixture of sulfates below 500°C". However, it should be noted that transformation and decomposition of kröhnkite revealed in the course of our HTXRD study is different as reported below. Kröhnkite-type compounds with various octahedrally coordinated cations and $T^{6+}O_4$ (T^{6+} = S, Cr and Se) groups are abundant in both minerals and synthetic compounds (Driscoll *et al*., 2016; Marinova *et al*., 2015; Siidra *et al*., 2014; Barpanda *et al*., 2014; Saha *et al*., 2011; Yang *et al*., 2011; Stoilova *et al*., 2009*a*,*b*; Wierzbicka-Wieczorek *et al*., 2008; Behera and Rao, 2006; Kolitsch and Fleck, 2005, 2006; Fleck and Kolitsch, 2003; Wildner and Stoilova, 2003; Pasha *et al*., 2003; Fleck *et al*., 2002*a*,*b*).

The present paper reports and discusses the results of HTXRD, thermal expansion and dehydration/hydration studies on kröhnkite from La Vendida mine, Antofagasta Region, Chile, and on the new mineral species saranchinaite, $Na_2Cu(SO_4)_2$. The latter was discovered by O.I.S. and E.A.L. in a fumarole at the Naboko scoria cone of the Tolbachik Fissure eruption that occurred in 2012–2013. The structural characterization of saranchinaite presented here has allowed us to characterize the dehydration and rehydration behaviour of kröhnkite. The new exhalative mineral was named saranchinaite (Cyrillic: саранчинаит) in honour of Prof. Galina M. Saranchina (1911–2004), a Russian petrologist who worked at the Department of Petrology, St. Petersburg State University, Russia. Besides her many scientific achievements in the field of metamorphic petrology she was an outstanding lecturer of petrology at the SPbSU and taught many generations of geoscientists including four co-authors (O.I.S., E.V.N., A.E.Y. and S.K.F.) of this paper. Both, the new mineral and its name have been approved by the IMA Commission on New Minerals, Nomenclature and Classification (IMA2015-019). The type specimen is deposited in the collections of the Mineralogical Museum, St Petersburg State University, St Petersburg, Russia, catalogue number 19639.

Occurrence and general appearance

Saranchinaite

Saranchinaite is formed as a product of fumarolic activity, probably by direct deposition as sublimate from volcanic gases. The holotype material was collected in the fumarole located at the Naboko

https://doi.org/10.1180/minmag.2017.081.037 Published online by Cambridge University Press

scoria cone (55°46′ N, 160°19′E, 1650 m a.s.l.) of the Tolbachik Fissure eruption that occurred in 2012–2013 on the south slope of the Ploskiy Tolbachik volcano, Kamchatka, Far-Eastern Region, Russia. The temperature of the gas at the sampling location was ~600°C. At the type locality saranchinaite is associated closely with euchlorine, $KNaCu_3(SO_4)_3O$ (Fig. 1*a*) and anhydrite. Other associated minerals are itelmenite $Na_4Mg_3Cu_3(SO_4)_8$ (Nazarchuk *et al*., 2018), hermannjahnite $CuZn(SO_4)_2$ (Siidra *et al*., 2018), chalcocyanite $CuSO_4$, thénardite Na_2SO_4, aphthitalite $K_3Na(SO_4)_2$ and hematite Fe_2O_3. Euchlorine and, surprisingly, saranchinaite appeared to be the most abundant Cu-sulfate minerals in the fumarole of Naboko cone. Thus it was decided to give the name of 'Saranchinaitovaya' to this fumarole. After the discovery of saranchinaite many similar looking samples in Cu-sulfate associations were checked from fumaroles of the Second Scoria Cone and perfect crystalline aggregates of sky-blue colour (Fig. 1*b*) were found to be very common. The reason why anhydrous saranchinaite has not been determined previously in the extremely rich mineral diversity of the fumaroles of the Second Scoria Cone is most probably due to its indistinguishability from hydrous kröhnkite during the preliminary qualitative microprobe examination of mineral samples. Instead we used single-crystal X-ray analysis for the primary examination of crystalline material from the exhalative mineral assemblages and this enabled us to discriminate between hydrous kröhnkite and the anhydrous new mineral saranchinaite.

Saranchinaite occurs typically as druses with crystals up to 0.1 mm, as spherolites or irregularly shaped grains, or in the form of microcrystalline masses. The colour of saranchinaite (Fig. 1*a*,*b*) is somewhat variable: very light-blue or nearly white in polycrystalline masses to sky-blue in crystalline aggregates. The streak is white. The lustre is vitreous. The mineral is transparent in individual grains and translucent in aggregates. Saranchinaite is brittle. Cleavage or parting has not been observed. The fracture is uneven. Hardness and density could not be measured because of the very small size of individual grains and the porosity of the aggregates. The density calculated on the basis of the empirical formula of the holotype is 2.937 g cm^{-3}. Saranchinaite is optically biaxial (+), $\alpha = 1.517(2)$, $\beta = 1.531(2)$ and $\gamma = 1.559(2)$ (589 nm) with $2V_{calc.} = 71.6°$. Saranchinaite appears light grey and non-pleochroic under the microscope. The Gladstone-Dale compatibility index, $1 - (K_p/K_c) = -0.025$, is excellent (Mandarino, 1981).

Kröhnkite

Well-crystallized greenish-blue kröhnkite samples (Fig. 1*c*) used for the HTXRD studies were collected in 2016 at the abandoned open pit of the La Vendida copper mine situated ~3 km WNW of the Sierra Gorda village, Antofagasta Region, Atacama Desert, Chile. Kröhnkite is also a common mineral from various fumaroles of the Second Scoria cone of the Northern Breakthrough of the Great Tolbachik Fissure eruption formed by alteration of Cu-sulfate mineral assemblages by air moisture and rain.

Chemical data for saranchinaite

Saranchinaite is water soluble and sensitive to moisture content in air. It transforms into kröhnkite after one week of exposure in open air at 87% relative humidity and 25°C. Therefore, all the samples were hermetically packed on-site immediately after collecting and isolated to avoid any contact with the atmosphere. The heating of the kröhnkite mineral sample up to 270°C was performed after the determination of the transformation temperature by HTXRD (see below). The transformation of kröhnkite powder samples into saranchinaite is accompanied by colour change from greenish-blue (Fig. 1*d*) to light-blue (Fig. 1*e*). No other intermediate phases are formed during this process as judged by powder XRD under controlled temperature conditions. In a humid atmosphere the obtained saranchinaite reverts back into kröhnkite (Fig. 1*f*).

Three crystals of saranchinaite checked previously by single-crystal XRD were mounted in epoxy resin and polished with oil suspension resulting in areas of ~40 μm × 40 μm. Ten spot analyses on the grains were obtained using a JEOL Superprobe 733 scanning electron microscope equipped with an Oxford Instruments INCA Energy Dispersive Spectrometer housed in the Fersman Mineralogical Museum, Russia. The electron beam accelerating voltage was 20 kV and the electron beam current 2 nA, measured with a Faraday cup. X-ray acquisition live-time was 30 s. System calibration was performed on Ni. The mineral is unstable under the focused electron beam with strong sodium loss during analysis and, therefore, a defocused beam (5 μm) was used for

https://doi.org/10.1180/minmag.2017.081.037 Published online by Cambridge University Press

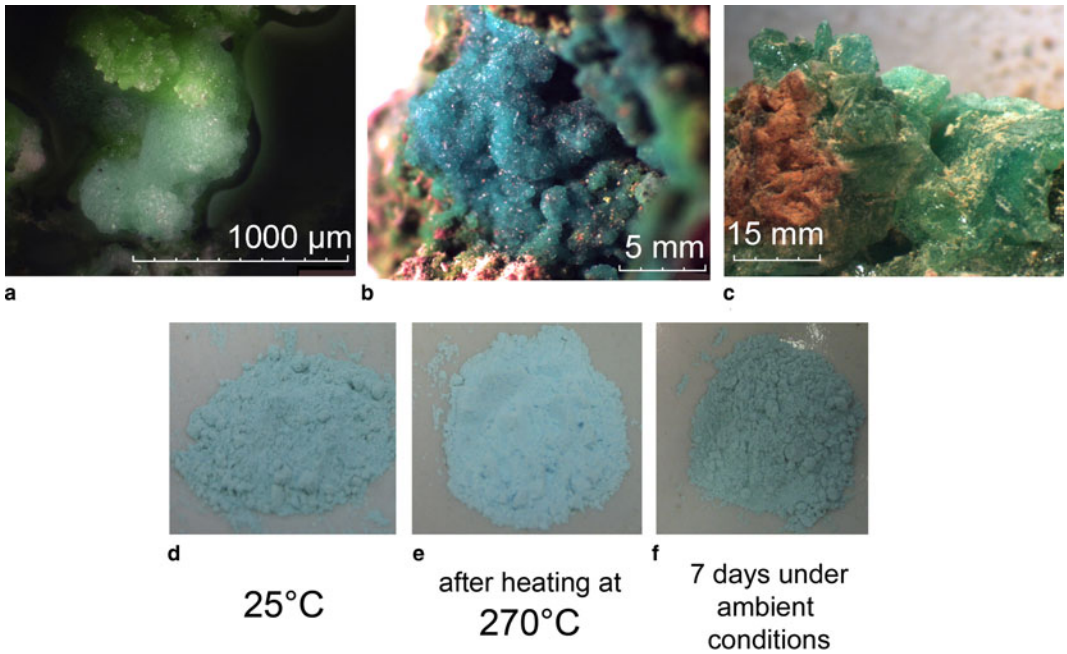

FIG. 1. (*a*) The holotype specimen of saranchinaite (light-blue) with euchlorine (green) from the Saranchinaitovaya fumarole, Naboko scoria cone, Tolbachik Fissure eruption; (*b*) the cotype specimen of saranchinaite from the Yadovitaya fumarole, Second scoria cone, Northern Breakthrough, Great Tolbachik Fissure eruption; (*c*) greenish-blue crystals of kröhnkite from La Vendida mine; (*d*) dehydration and transformation of polycrystalline sample of ground kröhnkite into saranchinaite by (*e*) heating to 270°C and (*f*) subsequent re-hydration back into kröhnkite after 7 days in air at relative humidity of 87% and 25°C.

analyses. X-ray matrix correction was carried out using the XPP routine implemented in the INCA software of Oxford Instruments. No elements with $Z \geq 9$ other than those reported in Table 1 were detected. The empirical formula calculated on the basis of 8 O atoms per formula unit is $(Na_{1.81}K_{0.14}Ca_{0.01})_{\sum 1.96}(Cu_{0.95}Zn_{0.03})_{\sum 0.98}S_{2.01}O_8$. The simplified formula is $Na_2Cu(SO_4)_2$.

X-ray crystallography and crystal structure of saranchinaite

Powder XRD data for the holotype of saranchinaite were obtained using a Rigaku Ultima IV diffractometer at the Department of Crystallography, St. Petersburg State University, Russia. Data (in Å for Cu$K\alpha$) are given in Table 2. The unit-cell

TABLE 1. Analytical results (wt.%) for the holotype of saranchinaite from Saranchinaitovaya fumarole.

Constituent	Wt.%	Range	S.D.	Probe standard
Na_2O	18.38	17.19–18.99	0.55	omphacite USNM 110607
K_2O	2.23	1.50–3.23	0.53	microcline USNM 143966
CaO	0.16	0.00–0.29	0.08	anorthite USNM 137041
CuO	24.72	23.93–25.46	0.43	Cu
ZnO	0.78	0.30–1.09	0.23	Zn
SO_3	52.79	51.47–55.11	1.08	$SrSO_4$
Total	99.05	97.50–101.15		

S.D.: standard deviation

https://doi.org/10.1180/minmag.2017.081.037 Published online by Cambridge University Press

parameters were refined in the monoclinic unit cell, space group $P2_1$, a = 8.995(3), b = 15.599(6), c = 10.159(3) Å, β = 107.07(11)° and V = 1363(1) Å^3.

An equant crystal (Table 3) of saranchinaite was mounted on a Bruker APEX II DUO X-ray diffractometer operated at 50 kV and 40 mA and equipped with a micro-focus X-ray tube with an Mo anode at the Department of Crystallography, St. Petersburg State University, Russia. The data were integrated and corrected for absorption using a multi-scan type model with the Bruker programs *APEX* and *SADABS* (Bruker AXS Inc., Madison, Wisconsin, USA). More than a hemisphere of XRD data was collected with frame widths of 0.3° in ω, and with 15 s spent counting for each frame. The $|E^2-1|$ parameter of 0.733 clearly indicated high probability of a non-centrosymmetric space group, which was confirmed by the subsequent structure solution and refinement. The structure of saranchinaite was solved in the space group $P2_1$ by direct methods. The crystal structure was refined to R_1 = 0.030 by means of the *SHELX* software package (Sheldrick, 2015) on the basis of 3236

TABLE 2. Powder XRD data of saranchinaite (in Å for Cu$K\alpha$).

I_{meas}	d_{meas}	d_{calc}	hkl
42.42	**8.6182**	**8.6135**	**100**
25.65	8.2595	8.2445	011
59.88	**7.8278**	**7.8178**	**020**
47.27	**7.6711**	**7.6535**	**10$\bar{1}$**
49.82	**6.0911**	**6.0877**	**021**
15.22	5.3336	5.3286	111
39.55	4.8925	4.8848	10$\bar{2}$
33.42	4.8566	4.8515	002
46.4	**4.6342**	**4.6336**	**012**
40.17	4.5833	4.5888	121
10.9	4.4489	4.4509	20$\bar{1}$
25.36	4.1304	4.1223	022
12.59	3.8977	3.9089	040
18.6	3.8251	3.8267	20$\bar{2}$
100	**3.7648**	**3.7722**	**220**
45.47	3.5482	3.5511	032
11.02	3.4725	3.4777	211
11.83	3.4315	3.4371	22$\bar{2}$
25.12	3.3109	3.3199	230
30.89	3.2941	3.2955	11$\bar{3}$
35.11	3.2344	3.2344	003
9.21	3.1676	3.1673	013
25.11	3.0964	3.0957	12$\bar{3}$
22.49	3.0555	3.0595	132
23.64	2.8616	2.8674	30$\bar{2}$
39.23	2.8176	2.824	310
17.9	2.7886	2.7885	212
57.32	2.7294	2.7293	113
98.27	**2.7122**	**2.717**	**142**
34.03	2.6294	2.6337	15$\bar{2}$
64.54	**2.5353**	**2.5375**	**10$\bar{4}$**
21.96	2.5219	2.523	311
10.55	2.4869	2.4897	232
10.62	2.4163	2.4135	12$\bar{4}$
16.82	2.4031	2.4092	152
17.03	2.0243	2.0256	33$\bar{4}$
9.04	1.7805	1.7821	26$\bar{4}$
7.69	1.7693	1.7721	412

The strongest eight lines are given in bold

TABLE 3. Crystallographic data and refinement parameters for saranchinaite.

Crystal data	
Formula	$Na_{7.7}K_{0.3}Cu_4S_8O_{32}$
Crystal system	Monoclinic
Space group	$P2_1$
Unit-cell dimensions	
a (Å)	9.0109(5)
b (Å)	15.6355(8)
c (Å)	10.1507(5)
α (°)	90.00
β (°)	107.079(2)
γ (°)	90.00
Unit-cell volume (Å^3)	1367.06(12)
Z	2
Calculated density (g·cm^{-3})	2.970
Absorption coefficient (mm^{-1})	3.982
Crystal size (mm)	0.10 × 0.10 × 0.05
Data collection	
Temperature (K)	296(2)
Radiation, wavelength (Å)	Mo$K\alpha$, 0.71073
F(000)	1180.6
θ range (°)	2.099–22.691
h, k, l ranges	$-9 \le h \le 9$ $-16 \le k \le 16$ $-11 \le l \le 11$
Total reflections collected	10,024
Unique reflections (R_{int})	3642 (0.0394)
Unique reflections $F > 4\sigma(F)$	3236
Structure refinement	
Refinement method	Full-matrix least-squares on F^2
Weighting coefficients a, b	0.0281, 0.00
Data/restraints/parameters	3236/1/472
R_1 [$F > 4\sigma(F)$], wR_2 [$F > 4\sigma(F)$]	0.0295, 0.0580
R_2 all, wR_2 all	0.0381, 0.0610
Goof on F^2	0.965
Largest diff. peak and hole (e Å^{-3})	0.459, –0.465

https://doi.org/10.1180/minmag.2017.081.037 Published online by Cambridge University Press

independent reflections with $F > 4\sigma(F)$. Atom coordinates and displacement parameters are given in Table 4 and selected interatomic distances in Table 5.

There are four symmetrically independent Cu^{2+} sites in the structure of saranchinaite (Fig. 2*a*). All Cu–O bonds <3.0 Å were taken into consideration. All Cu atoms form four very strong Cu–O bonds ≤ 2 Å resulting in CuO_4 squares which are complemented by a fifth, longer bond of ~2.2–2.3 Å, thus forming CuO_5 tetragonal pyramids. The Cu(1) and Cu(4) sites form one additional weaker bond resulting in [4+1+1] CuO_6 octahedra strongly distorted by the Jahn-Teller effect. This type of coordination geometry of Cu^{2+} cations is rather common in minerals and inorganic materials (Burns and Hawthorne, 1995). By way of contrast, the Cu(2) and Cu(3) sites display a very unusual [4+1+2] Cu^{2+} coordination environment with two additional Cu–O bonds of ~2.9–3.0 Å, thus forming CuO_7 polyhedra. To the best of our knowledge, only two other examples of heptacoordinated Cu^{2+} are known, *viz*. in the high pressure phase (II) of $CuGeO_3$ (Yoshiasa *et al*., 2000) and in a Cu-based complex polymer (Nadeem *et al*., 2010). Thus saranchinaite is unique as a mineral and as an inorganic compound housing heptacoordinated Cu^{2+} under ambient conditions. We plan to study this phenomenon subsequently with pure synthetic material. We hypothesize that the marked non-centrosymmetry of saranchinaite is related to the particularities of the Cu coordination. The Cu(1)-centred polyhedra are isolated (Fig. 3*d*) from other CuO_n polyhedra, while Cu(2)- and Cu(3)-centred polyhedra share a common O(3) corner thus forming dimeric units. $Cu(4)O_6$ polyhedra share common apical O(31) atoms with $Cu(3)O_7$.

There are eight distinct S sites, each occupied by S^{6+} and coordinated tetrahedrally by four O atoms (Table 5). The average S–O bond-lengths, 1.47–1.48 Å, are consistent with the average value of 1.475 Å given for sulfate minerals in general (Hawthorne *et al*., 2000).

Each of the eight independent Na sites in the structure is fully occupied by Na^+ cations except for Na(5) which is partly substituted for K^+. The details on coordination of the Na sites can be found in Table 5. Coordination numbers of Na sites are different and the following polyhedra are formed: $Na(1)O_8$, $Na(2)O_6$, $Na(3)O_6$, $Na(4)O_7$, $Na(5)O_6$, $Na(6)O_7$, $Na(7)O_6$ and $Na(8)O_6$.

Bond-valence calculations were performed using bond-valence parameters taken from Brese and O'Keeffe (1991) for the Na–O, Cu–O and S–O bonds. The results are presented in Table 6. As can be seen, there is general agreement between the expected and calculated oxidation states for all atomic sites. Note, Cu(2) and Cu(3) sites appear to be slightly overbonded with the bond-valence sums of 2.20 and 2.15 vu (valence units), respectively.

The polyhedra $Cu(2)O_7$, $Cu(3)O_7$ and $Cu(4)O_6$ share all of the oxygen apices with SO_4 tetrahedra (Fig. 2*b*) thus forming slightly corrugated layers stacked along [100] (Fig. 3*b*). For the sake of clarity CuO_5 (4+1) pyramids taking into account only the strongest Cu–O bonds are shown in Figs 2 and 3. Layers are linked into a rigid 3*D* $[Cu_4(SO_4)_8]^{8-}$ framework by $Cu(1)O_5$ pyramids acting as pillars (Fig. 3*a*). The complex 3*D* system of channels is occupied by Na (and minor K) atoms. In turn NaO_n polyhedra share common edges and corners thus also forming a 3*D* architecture. The structural topology of the $[Cu_4(SO_4)_8]^{8-}$ framework in saranchinaite is unique and has not been observed before.

High-temperature powder XRD study of kröhnkite and saranchinaite

The thermal behaviour of kröhnkite (Fig. 4) and saranchinaite (Fig. 5) was studied in air by means of a Rigaku Ultima X-ray diffractometer (Cu*K*α radiation) equipped with a high-temperature camera Rigaku HTA 1600. The samples were prepared from heptane suspension on Pt–Rh plates. Temperature steps were 25°C in the range 25–700°C (Fig. 4*a*) for the first full measurement of kröhnkite and detailed additional measurements were undertaken in the range 150–250°C with steps of 5°C (Fig. 4*b*). X-ray diffraction patterns for saranchinaite were obtained in the range 25–900°C with step size 25°C. Unit-cell parameters at different temperatures were refined by least-squares methods. The main coefficients of the thermal expansion tensor were determined using linear approximation of temperature dependences by the *ThetaToTensor* program (Firsova *et al*., 2011). Temperatures of the decomposition of kröhnkite and saranchinaite were estimated as the mean temperature between the two corresponding HTXRD experiments where the diffraction pattern changes. i.e. where peaks of another phase appear.

Kröhnkite

The evolution of the powder diffraction pattern of kröhnkite as function of temperature is shown in

https://doi.org/10.1180/minmag.2017.081.037 Published online by Cambridge University Press

TABLE 4. Atomic coordinates and displacement parameters (Å^2) for saranchinaite.

Atom	*x/a*	*y/b*	*z/c*	U_{eq}	U^{11}	U^{22}	U^{33}	U^{23}	U^{13}	U^{12}
Cu1	0.65627(16)	0.08103(8)	0.67841(14)	0.0171(4)	0.0151(9)	0.0198(8)	0.0170(8)	0.0030(7)	0.0056(6)	0.0004(6)
Cu2	0.93026(15)	0.31758(8)	0.01360(13)	0.0152(4)	0.0156(9)	0.0140(8)	0.0161(8)	0.0022(7)	0.0047(6)	0.0001(6)
Cu3	0.91226(16)	0.53157(9)	0.96663(13)	0.0158(3)	0.0151(8)	0.0132(7)	0.0192(8)	−0.0004(7)	0.0052(6)	0.0009(6)
Cu4	0.89712(16)	0.52838(9)	0.47971(13)	0.0170(3)	0.0148(8)	0.0190(7)	0.0175(7)	−0.0022(7)	0.0055(6)	0.0013(7)
S1	0.6078(3)	0.41691(19)	0.9030(3)	0.0154(7)	0.0133(17)	0.0171(16)	0.0164(17)	0.0014(14)	0.0050(13)	0.0004(13)
S2	0.7645(4)	0.70721(18)	0.9179(3)	0.0147(7)	0.0145(18)	0.0142(16)	0.0155(16)	0.0015(14)	0.0043(13)	−0.0002(13)
S3	0.0517(3)	0.45475(17)	0.2826(3)	0.0147(7)	0.0165(18)	0.0151(17)	0.0125(16)	0.0022(14)	0.0044(13)	0.0026(13)
S4	0.6738(3)	0.68231(18)	0.4064(3)	0.0154(7)	0.0141(18)	0.0175(16)	0.0149(16)	0.0031(15)	0.0047(13)	0.0003(14)
S5	0.7797(3)	0.13222(19)	0.4380(3)	0.0162(7)	0.0163(17)	0.0183(18)	0.0143(15)	0.0033(15)	0.0048(12)	0.0009(14)
S6	0.9782(3)	0.40443(18)	0.7622(3)	0.0171(7)	0.0186(18)	0.0185(18)	0.0148(16)	−0.0012(15)	0.0059(13)	0.0005(14)
S7	0.4327(3)	−0.05445(18)	0.6585(3)	0.0180(7)	0.0172(18)	0.0176(18)	0.0194(17)	0.0059(15)	0.0055(14)	0.0011(13)
S8	0.7950(3)	0.14313(18)	0.9962(3)	0.0139(7)	0.0143(18)	0.0137(16)	0.0139(15)	−0.0014(14)	0.0048(12)	0.0001(13)
Na1	0.2844(5)	0.4230(3)	0.0517(5)	0.0281(12)	0.023(3)	0.030(3)	0.036(3)	−0.001(2)	0.016(2)	−0.005(2)
Na2	0.2897(5)	0.4116(3)	0.6167(5)	0.0268(12)	0.020(3)	0.032(3)	0.026(3)	0.001(3)	0.002(2)	−0.001(2)
Na3	0.9760(6)	0.6831(3)	0.2462(5)	0.0255(12)	0.022(3)	0.029(3)	0.024(3)	0.001(2)	0.003(2)	−0.003(2)
Na4	0.6173(5)	0.5508(3)	0.6641(4)	0.0266(12)	0.023(3)	0.037(3)	0.019(2)	−0.003(2)	0.006(2)	−0.006(2)
Na5*	0.3608(5)	0.8037(2)	0.4244(4)	0.0336(17)	0.031(3)	0.023(3)	0.047(3)	−0.001(2)	0.013(2)	0.0017(19)
Na6	0.6022(5)	0.5866(3)	0.0853(4)	0.0246(11)	0.024(3)	0.033(3)	0.018(2)	−0.001(2)	0.009(2)	0.000(2)
Na7	0.9408(5)	0.7261(3)	0.6701(4)	0.0261(12)	0.027(3)	0.032(3)	0.018(3)	−0.006(2)	0.003(2)	−0.004(2)
Na8	0.6277(5)	0.2695(3)	0.1551(4)	0.0231(11)	0.018(3)	0.030(3)	0.020(2)	0.000(2)	0.005(2)	0.002(2)
O1	0.8784(8)	0.0605(4)	0.0320(7)	0.0165(19)	0.014(5)	0.006(4)	0.030(5)	0.002(4)	0.008(4)	0.001(3)
O2	0.0089(9)	0.3678(5)	0.2324(7)	0.0177(19)	0.021(5)	0.016(4)	0.015(4)	−0.001(4)	0.003(3)	0.001(4)
O3	0.9683(8)	0.4179(5)	0.9124(7)	0.0167(18)	0.025(5)	0.019(4)	0.009(4)	0.003(4)	0.011(3)	0.000(4)
O4	0.8557(9)	0.6435(5)	0.0206(7)	0.0189(19)	0.020(5)	0.018(4)	0.016(4)	−0.001(4)	0.001(3)	0.003(4)
O5	0.5025(9)	0.6759(5)	0.3824(8)	0.0210(19)	0.015(5)	0.024(4)	0.021(4)	−0.002(4)	0.001(3)	0.001(4)
O6	0.8492(8)	0.7906(4)	0.9537(7)	0.0188(19)	0.013(5)	0.017(5)	0.028(5)	−0.005(4)	0.009(4)	−0.003(4)
O7	0.6926(9)	0.5012(4)	0.9151(8)	0.022(2)	0.019(5)	0.009(4)	0.035(5)	−0.001(4)	0.007(4)	−0.006(4)
O8	0.6132(9)	0.7157(5)	0.9367(8)	0.025(2)	0.012(5)	0.031(5)	0.033(5)	0.010(4)	0.009(4)	0.002(4)
O9	0.8844(9)	0.4734(5)	0.6821(7)	0.023(2)	0.025(5)	0.029(5)	0.015(5)	0.006(4)	0.005(4)	0.005(4)
O10	0.7181(9)	0.6689(5)	0.2825(7)	0.024(2)	0.027(5)	0.032(5)	0.014(4)	0.003(4)	0.005(4)	−0.001(4)
O11	0.7366(10)	0.2150(5)	0.3762(8)	0.024(2)	0.033(5)	0.017(5)	0.022(5)	0.007(4)	0.005(4)	0.004(4)
O12	0.7462(8)	0.6132(5)	0.5081(7)	0.0190(19	0.010(5)	0.026(5)	0.023(4)	0.002(4)	0.007(3)	0.010(3)
O13	0.7147(9)	0.3497(4)	0.9841(8)	0.022(2)	0.020(5)	0.018(5)	0.031(5)	0.013(4)	0.009(4)	0.011(4)
O14	0.5111(8)	0.0176(4)	0.7504(7)	0.0185(18)	0.016(4)	0.013(4)	0.028(4)	0.001(4)	0.008(3)	−0.002(4)
O15	0.2100(9)	0.4736(5)	0.2733(8)	0.0206(19)	0.016(5)	0.016(4)	0.032(5)	0.000(4)	0.011(4)	−0.002(4)

(continued)

TABLE 4. (*contd*.)

Atom	*x*/*a*	*y*/*b*	*z*/*c*	U_{eq}	U^{11}	U^{22}	U^{33}	U^{23}	U^{13}	U^{12}
O16	0.0553(8)	0.4586(4)	0.4309(7)	0.0157(18)	0.015(5)	0.023(4)	0.010(4)	0.004(4)	0.006(3)	0.006(3)
O17	0.9113(10)	0.3202(5)	0.7227(8)	0.033(2)	0.054(6)	0.017(5)	0.027(5)	−0.014(4)	0.010(4)	−0.004(5)
O18	0.9401(9)	0.1129(5)	0.4307(8)	0.023(2)	0.019(5)	0.027(5)	0.029(5)	0.008(4)	0.015(4)	0.007(4)
O19	0.7916(8)	0.1393(5)	0.5893(7)	0.0173(18	0.015(5)	0.024(5)	0.015(4)	0.006(4)	0.008(3)	−0.001(4)
O20	0.5541(9)	0.3954(5)	0.7572(7)	0.029(2)	0.032(6)	0.034(5)	0.015(4)	−0.006(4)	−0.003(4)	0.001(4)
O21	0.1391(9)	0.4091(6)	0.7681(8)	0.030(2)	0.024(5)	0.047(6)	0.025(5)	0.000(5)	0.015(4)	0.008(4)
O22	0.6444(8)	0.1357(5)	0.0152(7)	0.024(2)	0.011(5)	0.031(5)	0.029(5)	−0.002(4)	0.005(4)	0.000(4)
O23	0.7921(9)	0.1668(5)	0.8547(7)	0.023(2)	0.023(5)	0.031(5)	0.015(4)	0.002(4)	0.004(4)	0.004(4)
O24	0.7619(9)	0.6789(5)	0.7812(7)	0.025(2)	0.028(5)	0.031(5)	0.014(4)	−0.005(4)	0.003(4)	−0.004(4)
O25	0.4862(9)	−0.1344(5)	0.7259(8)	0.025(2)	0.023(5)	0.019(5)	0.033(5)	0.001(4)	0.008(4)	0.002(4)
O26	0.8866(8)	0.2103(4)	0.0936(7)	0.0154(18)	0.018(5)	0.011(4)	0.014(4)	−0.004(3)	0.000(3)	−0.007(3)
O27	0.4814(9)	0.4290(6)	0.9625(8)	0.031(2)	0.024(5)	0.037(5)	0.037(6)	0.006(5)	0.019(4)	0.003(4)
O28	0.7250(9)	0.7656(4)	0.4675(7)	0.021(2)	0.027(5)	0.013(4)	0.020(4)	−0.009(4)	0.003(4)	−0.007(4)
O29	0.4692(9)	−0.0472(5)	0.5265(8)	0.030(2)	0.025(5)	0.051(6)	0.020(5)	0.010(5)	0.015(4)	0.014(4)
O30	0.2643(9)	−0.0470(5)	0.6372(8)	0.024(2)	0.013(5)	0.031(5)	0.026(5)	0.009(4)	0.004(4)	0.006(4)
O31	0.9426(8)	0.5184(5)	0.2040(7)	0.0208(19)	0.022(5)	0.025(5)	0.017(4)	0.003(4)	0.008(3)	0.006(4)
O32	0.6709(9)	0.0647(5)	0.3781(7)	0.024(2)	0.024(5)	0.025(5)	0.021(4)	−0.003(4)	0.005(4)	−0.006(4)

*$Na_{0.71(2)}K_{0.29(2)}$

TABLE 5. Selected interatomic distances in the structure of saranchinaite.

Cu1–O19	1.945(7)	Cu3–O1	1.936(7)	Na1–O27	2.219(9)	Na5–O5	2.475(8)
Cu1–O14	1.947(7)	Cu3–O4	1.946(7)	Na1–O6	2.388(9)	Na5–O17	2.482(9)
Cu1–O5	2.027(8)	Cu3–O7	1.952(7)	Na1–O1	2.600(8)	Na5–O29	2.622(9)
Cu1–O15	2.041(7)	Cu3–O3	1.970(7)	Na1–O15	2.650(9)	Na5–O20	2.622(9)
Cu1–O23	2.283(8)	Cu3–O31	2.352(7)	Na1–O25	2.727(9)	Na5–O11	2.799(9)
Cu1–O29	2.777(9)	Cu3–O9	2.968(7)	Na1–O14	2.728(9)	Na5–O19	2.898(8)
		Cu3–O24	3.030(7)	Na1–O3	2.785(9)	<Na5–O>	2.65
Cu2–O13	1.943(7)			Na1–O21	2.799(10)		
Cu2–O26	1.954(7)	Cu4–O16	1.971(7)	<Na1–O>	2.61	Na6–O22	2.288(8)
Cu2–O3	1.959(7)	Cu4–O30	1.975(7)			Na6–O10	2.350(9)
Cu2–O6	1.963(7)	Cu4–O12	1.980(7)	Na2–O21	2.331(9)	Na6–O14	2.447(8)
Cu2–O2	2.264(7)	Cu4–O18	1.985(7)	Na2–O20	2.404(9)	Na6–O7	2.502(9)
Cu2–O17	2.908(8)	Cu4–O9	2.261(7)	Na2–O32	2.417(9)	Na6–O8	2.539(9)
Cu2–O23	2.921(8)	Cu4–O31	2.950(7)	Na2–O28	2.428(9)	Na6–O4	2.706(9)
				Na2–O16	2.494(8)	Na6–O27	2.831(10)
S1–O27	1.449(8)	S5–O11	1.441(8)	Na2–O29	3.017(9)	<Na6–O>	2.52
S1–O20	1.455(8)	S5–O32	1.448(8)	<Na2–O>	2.52		
S1–O13	1.498(8)	S5–O18	1.499(8)			Na7–O24	2.340(9)
S1–O7	1.510(8)	S5–O19	1.512(7)	Na3–O4	2.312(8)	Na7–O2	2.414(9)
<S1–O>	1.48	<S5–O>	1.48	Na3–O17	2.352(10)	Na7–O18	2.445(9)
				Na3–O19	2.364(8)	Na7–O26	2.458(8)
S2–O8	1.437(8)	S6–O21	1.436(8)	Na3–O10	2.468(10)	Na7–O28	2.459(9)
S2–O24	1.450(8)	S6–O17	1.455(9)	Na3–O23	2.596(9)	Na7–O12	2.683(9)
S2–O6	1.500(8)	S6–O9	1.460(8)	Na3–O31	2.614(10)	<Na7–O>	2.47
S2–O4	1.500(8)	S6–O3	1.567(7)	<Na3–O>	2.45		
<S2–O>	1.47	<S6–O>	1.48			Na8–O8	2.258(9)
				Na4–O29	2.410(9)	Na8–O11	2.330(9)
S3–O31	1.460(7)	S7–O25	1.439(8)	Na4–O12	2.426(9)	Na8–O25	2.345(9)
S3–O2	1.464(8)	S7–O30	1.473(8)	Na4–O24	2.493(9)	Na8–O13	2.449(9)
S3–O15	1.487(8)	S7–O29	1.475(8)	Na4–O32	2.514(9)	Na8–O22	2.558(9)
S3–O16	1.497(7)	S7–O14	1.500(8)	Na4–O7	2.557(9)	Na8–O26	2.747(9)
<S3–O>	1.48	<S7–O>	1.47	Na4–O9	2.652(9)	<Na8–O>	2.45
				Na4–O20	2.726(9)		
S4–O10	1.442(8)	S8–O22	1.430(8)	<Na4–O>	2.54		
S4–O28	1.458(7)	S8–O23	1.476(8)				
S4–O5	1.494(8)	S8–O1	1.485(7)				
S4–O12	1.505(8)	S8–O26	1.510(7)				
<S4–O>	1.47	<S8–O>	1.48				

Fig. 4. With increasing temperature, the pattern does not undergo significant changes. The reflections of kröhnkite gradually start to disappear at ~170°C (Fig. 4*b*). At this temperature, peaks of saranchinaite appear indicating the dehydration of kröhnkite. Note that the chemical formulae of both minerals are identical except of H_2O molecules in kröhnkite. Full dehydration of kröhnkite and transformation into saranchinaite is completed at 200°C. No peaks corresponding to other phases could be observed. The temperature dependence of the cell parameters (Supplementary Fig. 1S) of kröhnkite can be described by the following linear functions:

$$a_t = 5.807(2) + 0.252(2) \times 10^{-3}t$$
$$b_t = 12.666(1) + 0.341(3) \times 10^{-3}t$$
$$c_t = 5.521(5) + 0.122(2) \times 10^{-3}t$$
$$\beta_t = 108.446(6) + 0.026(7) \times 10^{-3}t$$

$V_t = 385.21(2) + 29(2) \times 10^{-3}t$, where t is a temperature. Upon heating, the unit cell is expanding along all crystallographic axes.

The following values of the principal eigenvalues of the thermal expansion tensor of a unit cell at 25°C were obtained: $\alpha_a \approx \alpha_{11} = 44.6 \times 10^{-6}$ °C^{-1},

https://doi.org/10.1180/minmag.2017.081.037 Published online by Cambridge University Press

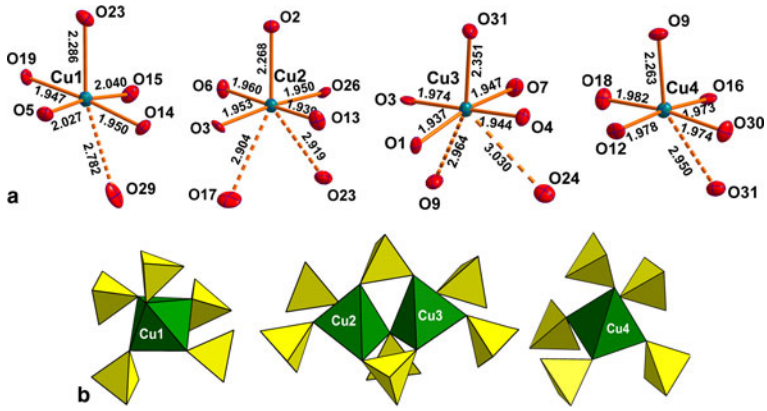

FIG. 2. (*a*) Coordination of Cu^{2+} cations and (*b*) interconnection of CuO_5 pyramids (taking into account only strong Cu-O bonds) with sulfate tetrahedra in the structure of saranchinaite.

$\alpha_b = \alpha_{22} = 24.2 \times 10^{-6}$ °C^{-1}, $\alpha_c \approx \alpha_{33} = 6.4 \times 10^{-6}$ °C^{-1}, $\alpha_V = 75.4 \times 10^{-6}$ °C^{-1} and μ (α_{II}^a) = 8.9°. The structure of kröhnkite (Hawthorne and Ferguson, 1975) (Fig. 6) is based on chains of SO_4 tetrahedra and $CuO_4(H_2O)_2$ octahedra extending along the *c* axis. The chains are linked by Na^+ cations each coordinated by seven O atoms. The $CuO_4(H_2O)_2$ octahedra show typical Jahn-Teller distorted [4+2] geometry. NaO_7 polyhedra share common edges thus forming dimers (Fig. 6*c*) which are interconnected eventually into layers via common corners. The strongly anisotropic character (Fig. 7) of the thermal expansion of kröhnkite remains essentially unchanged up to its decomposition (Table 7). The highest α_a expansion is observed perpendicular to the Na interlayer (Fig. 6*a*), whereas minimal α_c thermal expansion occurs in the direction of the rigid $[Cu(SO_4)_2(H_2O)_2]^{2-}$ chains (Fig. 6*b*). Rather strong bonding between Na-centred polyhedra in the interlayer is reflected in the α_b expansion value.

Saranchinaite

The thermal expansion and decomposition of saranchinaite (Table 8; Figs 3, 8) is significantly more complex than that of kröhnkite. It is identical for both saranchinaite from Tolbachik and saranchinaite obtained by dehydration of kröhnkite. The results reported below were obtained from saranchinaite found in the Saranchinaitovaya fumarole. Saranchinaite is stable up to 475°C when it starts to decompose into tenorite, thénardite and an unidentified phase.

There is a continuous expansion of the unit-cell volume (Supplementary Fig. 2S), associated with a volume thermal expansion coefficient (Table 8). The expansion of saranchinaite is strongly anisotropic, such that the *a*, *b* and *c* axes expand with increasing temperature:

$$a_t = 8.991(1) + 0.109(1) \times 10^{-3} t + 0.186(3) \times 10^{-6} t^2$$

$$b_t = 15.586(4) + 0.342(3) \times 10^{-3} t - 0.216(7) \times 10^{-6} t^2$$

$$c_t = 10.150(2) + 0.123(2) \times 10^{-3} t + 0.270(5) \times 10^{-6} t^2$$

$$\beta_t = 107.111(1) - 0.379(5) \times 10^{-3} t$$

$V_t = 1357.75(4) + 87(2) \times 10^{-3} t$, where *t* is a temperature.

At 25°C α_{11} and α_{22} are very similar but expansion behaviour changes with the temperature rise. The strongest expansion of saranchinaite is observed in the direction of the bisector of the β angle (corresponding to α_{11}), whereas less expansion occurs in the direction of the perpendicular diagonal of the unit cell (α_{33}). This thermal behaviour can be explained on the basis of the considerations of the respective rigidity of structural units in saranchinaite. SO_4 tetrahedra and CuO_n polyhedra are the most rigid building units. The *b* axis is nearly parallel to the virtual Cu(2)–Cu(3) axis in dimers (Fig. 2*b*). These dimers

https://doi.org/10.1180/minmag.2017.081.037 Published online by Cambridge University Press

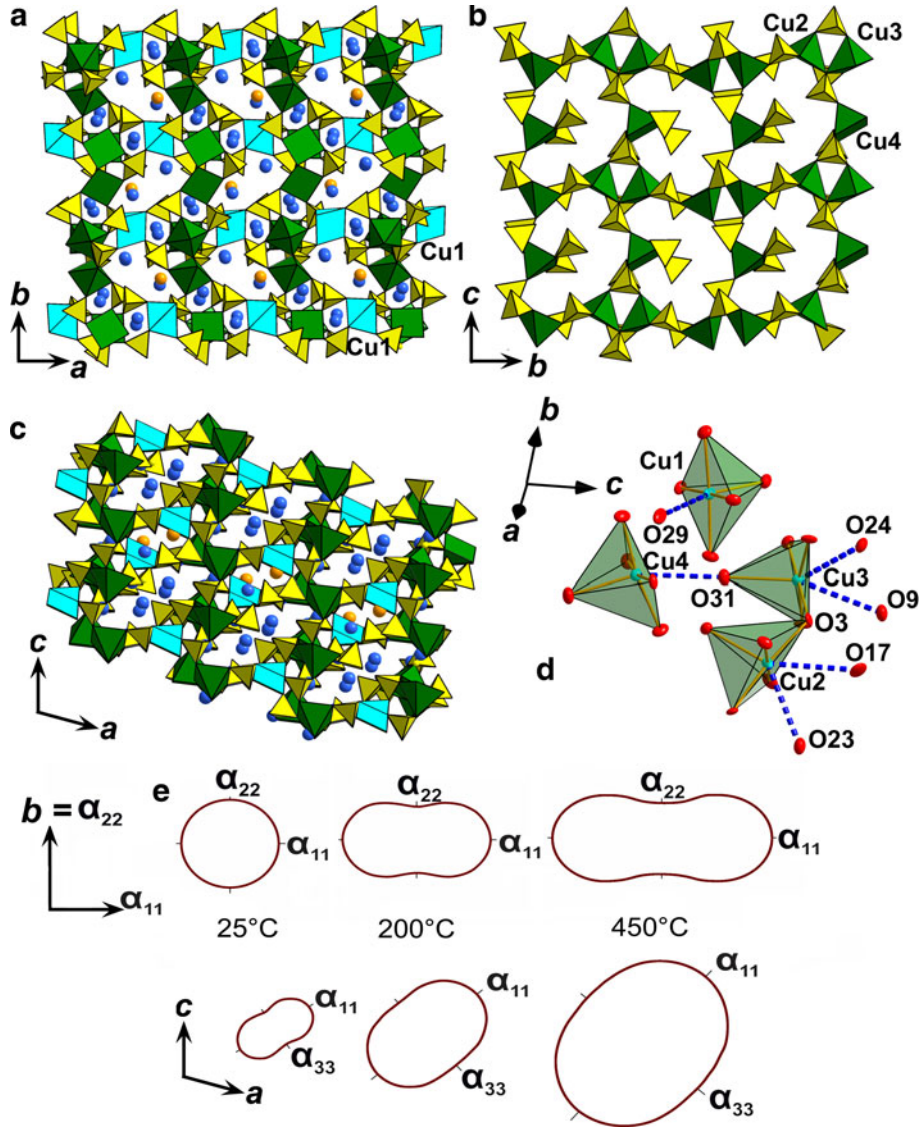

FIG. 3. General projection of the crystal structure of saranchinaite along the *c* (a) and *a* (b) and *b* (c) axis (Na5 sites are marked by orange and the remaining Na atoms are blue). The $[Cu_4(SO_4)_8]^{2-}$ framework consists of layers (*c*) formed by $Cu(2)O_5$, $Cu(3)O_5$, $Cu(4)O_5$ tetragonal pyramids and sulfate tetrahedra. Layers are interconnected *via* $Cu(1)O_5$ (marked by sky blue) tetragonal pyramids. (*d*) Orientation of weak Cu–O bonds (blue dotted lines) in the structure of saranchinaite. (*e*) Pole figures of the thermal expansion coefficients of saranchinaite at different temperatures.

are fixed rigidly by sulfate tetrahedra in between them. α_{22} expansion of the structure decreases significantly (Fig. 8, Table 8) with the temperature. α_{11} occurs in a direction nearly perpendicular to the Cu-sulfate layers formed by $Cu(2)O_7$, $Cu(3)O_7$ and $Cu(4)O_6$ (Fig. 3).

Final remarks

Saranchinaite represents a new structure type and has no direct synthetic analogues. Anhydrous compounds of composition $A_2Cu(SO_4)_2$ (A = Na, K, Rb and Cs) are unknown. The structural

https://doi.org/10.1180/minmag.2017.081.037 Published online by Cambridge University Press

TABLE 6. Bond-valence values (in valence units) for saranchinaite.

	O1	O2	O3	O4	O5	O6	O7	O8	O9	O10	O11	O12	O13	O14	O15	O16	O17
Cu1					0.39									0.48	0.38		
Cu2		0.21	0.47			0.46							0.49				0.06
Cu3	0.5		0.46	0.49			0.48		0.03								
Cu4									0.21			0.44				0.45	
S1							1.36						1.41				
S2				1.4		1.4		1.66									
S3		1.54													1.45	1.41	
S4					1.42					1.64		1.38					
S5											1.64						
S6			1.17						1.56								1.58
S7														1.4			
S8	1.46																
Na1	0.12		0.07			0.21								0.08	0.1		
Na2																0.15	
Na3				0.25						0.17							0.23
Na4							0.13		0.1			0.19					
Na5*					0.16						0.07						0.16
Na6				0.09			0.15	0.14		0.23				0.18			
Na7		0.19										0.09					
Na8								0.29			0.24		0.17				
Σ_vc	2.08	1.94	2.17	2.23	1.97	2.07	2.12	2.09	1.9	2.04	1.95	2.1	2.07	2.14	1.93	2.01	2.03

*$Na_{0.71(2)}K_{0.29(2)}$.

O18	O19	O20	O21	O22	O23	O24	O25	O26	O27	O28	O29	O30	O31	O32	Σ_va
	0.49				0.20						0.05				1.99
					0.03			0.48							2.20
						0.03							0.16		2.15
0.44												0.45	0.03		2.02
		1.58							1.6						5.95
						1.6									6.06
													1.56		5.96
										1.57					6.01
1.4	1.35													1.61	6.00
			1.66												5.97
							1.65				1.5	1.5			6.05
				1.69	1.49			1.36							6.00
			0.07				0.08		0.32						1.05
		0.2	0.24							0.18	0.04			0.19	1.00
	0.22				0.12								0.11		1.10
		0.08				0.15					0.19			0.15	0.99
	0.05	0.11									0.11				0.66
				0.27					0.06						1.12
0.18						0.23		0.17		0.17					1.03
				0.13			0.23	0.08							1.14
2.02	2.11	1.97	1.97	2.09	1.84	2.01	1.96	2.09	1.98	1.92	1.89	1.95	1.86	1.95	

https://doi.org/10.1180/minmag.2017.081.037 Published online by Cambridge University Press

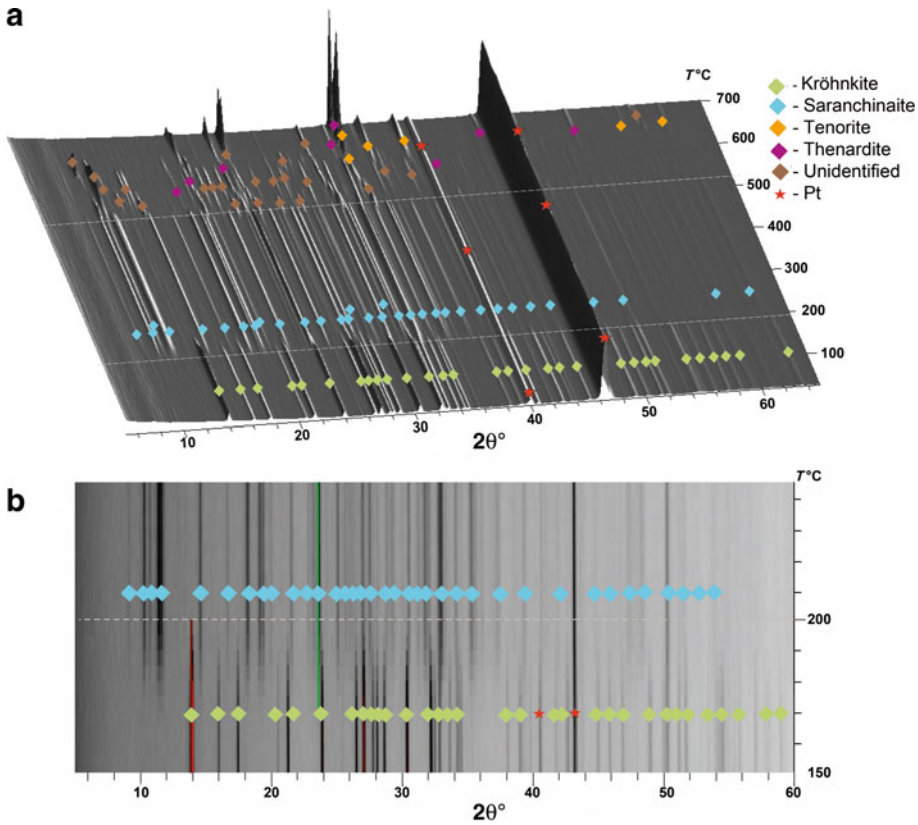

FIG. 4. Three-dimensional perspective plot showing all diffractograms of kröhnkite over 5–60°2θ with increasing temperature. The dashed white line indicates transformation of kröhnkite into saranchinaite in the range of 170–200°C.

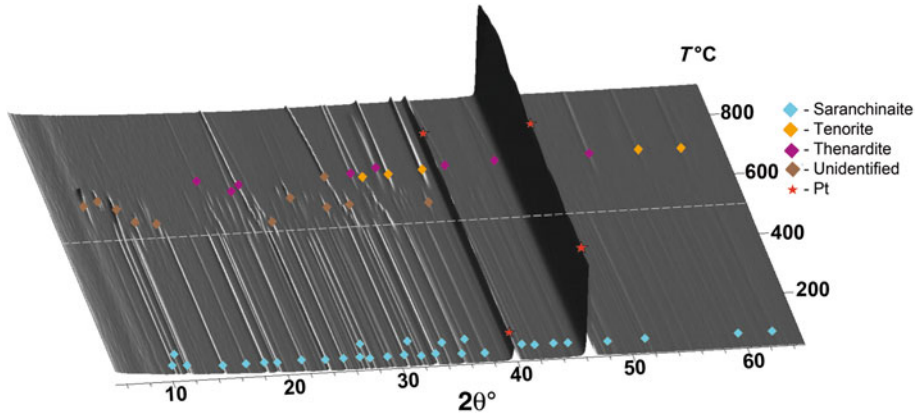

FIG. 5. Three-dimensional perspective plot showing all diffractograms of saranchinaite over 5–60°2θ with increasing temperature. The dashed white line indicates decomposition of saranchinaite into tenorite, thénardite and unidentified phase/phases at 520°C.

https://doi.org/10.1180/minmag.2017.081.037 Published online by Cambridge University Press

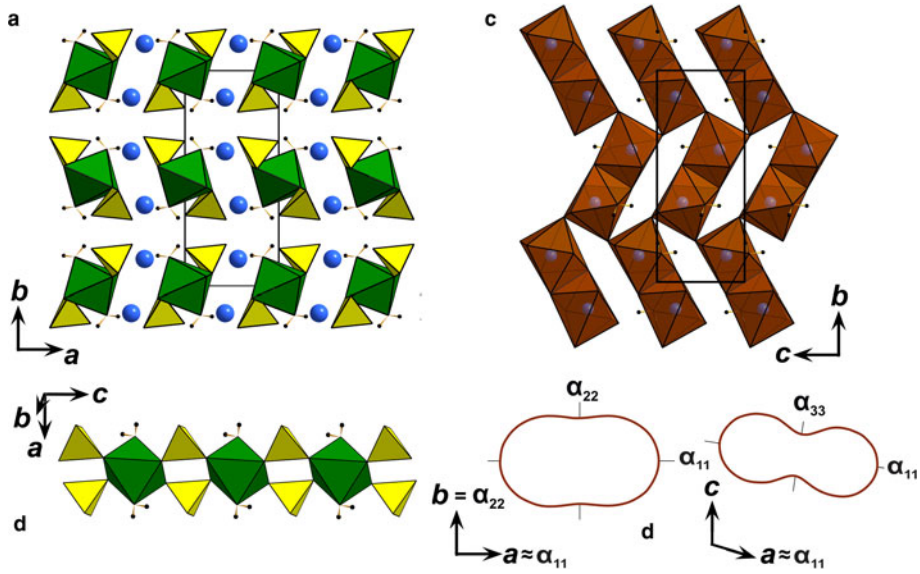

FIG. 6. (*a*) General projection of the crystal structure of kröhnkite (after Hawthorne and Ferguson, 1975) along the *c* axis (Na sites are marked by blue balls and H atoms are black). (*b*) $[Cu(SO_4)_2(H_2O)_2]^{2-}$ chains in the structure of kröhnkite. (*c*) Arrangement of NaO_7 polyhedra in the interlayer. (*d*) Pole figures of the thermal expansion coefficients of kröhnkite in *ba* and *ca* planes.

topologies of the high-temperature anhydrous mineral saranchinaite and of the low-temperature hydrated kröhnkite are unrelated; saranchinaite is significantly more complex than kröhnkite. Natrochalcite, $NaCu_2(SO_4)_2(OH)(H_2O)$ (Chevrier *et al*., 1993) is again structurally unrelated to saranchinaite, but is based on kröhnkite-type chains. 'Pure' Na–Cu sulfate minerals *sensu stricto* (i.e. minerals with independent crystallographic positions of Na and Cu) without additional cations and anions are unknown. The majority of Cu-containing sulfates of exhalative origin are K-dominant (Siidra *et al*., 2017). Saranchinaite is the second Na-dominant Cu-sulfate mineral observed in fumaroles of scoria cones on Tolbachik volcano. Recently, we have described another Cu sulfate which, however, contains additional oxygen atoms, *viz*. puninite, $Na_2Cu_3O(SO_4)_3$ from fumaroles of the Second Scoria cone. Kröhnkite is a very abundant mineral in altered mineral crusts of the Second Scoria cone and most probably the hydration product of saranchinaite.

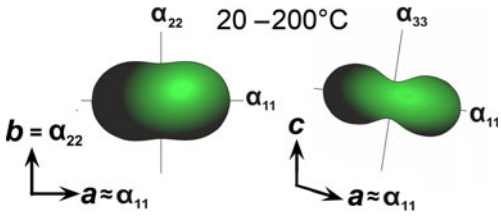

FIG. 7. Thermal expansion tensors for kröhnkite (see Table 8) in the range of 20–200°C.

High-temperature powder XRD studies show that kröhnkite starts decomposing at 170°C and at ~200°C full transformation into saranchinaite is achieved by losing all of the water content. Notably, during this transformation the '$Na_2Cu(SO_4)_2$' main part of the chemical formula is retained, despite the lack of direct structural relations between kröhnkite and saranchinaite. Kröhnkite crystals (Fig. 1*c*) have a greenish tint whereas saranchinaite is blue (Fig. 1*a*,*b*). The difference in colour may be the result of different coordination environments of Cu^{2+} cations in both crystal structures: [4+1+1] and [4+1+2] in saranchinaite, but [4+2] in kröhnkite.

The discovery of saranchinaite and the successful determination of its crystal structure may facilitate the structure determination of various kröhnkite-type materials (Driscoll *et al*., 2016; Barpanda *et al*., 2014; Saha *et al*., 2011; Behera and Rao, 2006; Pasha *et al*., 2003) from powder

https://doi.org/10.1180/minmag.2017.081.037 Published online by Cambridge University Press

TABLE 7. Values ($\times 10^{-6}$ °C^{-1}) of the principal eigenvalues of thermal expansion tensor of the unit cell of kröhnkite at different temperatures (T°C).

T	α_{11}	α_{22}	α_{33}	α_a	α_b	α_c	α_V
25	45.7	24.2	8.8	45(4)	24.16(10)	10(1)	79(4)
50	45.6	24.1	8.8	45(4)	24.15(10)	10(1)	79(4)
75	45.6	24.1	8.8	45(4)	24.14(10)	10(1)	79(4)
100	45.5	24.1	8.8	45(4)	24.12(10)	10(1)	78(4)
125	45.5	24.1	8.8	45(4)	24.11(10)	10(1)	78(4)
150	45.4	24.1	8.8	45(4)	24.09(10)	10(1)	78(4)
175	45.4	24.1	8.8	44(4)	24.08(10)	10(1)	78(4)

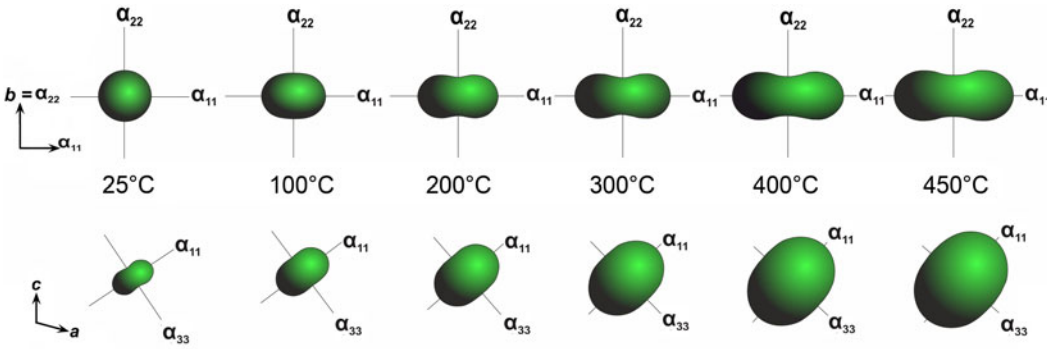

FIG. 8. Evolution of thermal expansion tensors of saranchinaite at different temperatures.

samples and the investigation of the physical properties of products of decomposition of others (Driscoll *et al*., 2016; Barpanda *et al*., 2014; Saha *et al*., 2011; Behera and Rao, 2006; Pasha *et al*., 2003). It should be noted that recently the transformation of kröhnkite-type $Na_2Mn(SO_4)_3{\cdot}2H_2O$ into an alluaudite-type structure has been reported (Marinova *et al*., 2015). This lends itself to the speculation that the transformation of kröhnkite-type materials into saranchinaite-type phases may be restricted to Cu-based compounds due to the Jahn-Teller effect on Cu^{2+}.

The observed complex character of thermal expansion in saranchinaite might be of special interest, given the high scientific interest in this phenomenon and its potential for practical applications in controlled thermal expansion composites. We have successfully synthesized the K-free $Na_2Cu(SO_4)_2$ analogue of saranchinaite. Magnetic properties as well as measurements of electrochemical

TABLE 8. Values ($\times 10^{-6}$ °C^{-1}) of the principal eigenvalues of thermal expansion tensor of the unit cell of saranchinaite at different temperatures (T°C).

T	α_{11}	α_{22}	α_{33}	α_a	α_b	α_c	α_V
25	17.1	16.0	8.8	12(1)	16(4)	12(2)	42(4)
100	20.7	14.3	12.4	15.2(7)	14(2)	15(1)	47(3)
200	25.5	12.0	17.1	19.5(3)	12.0(8)	20.7(6)	55(1)
300	30.3	9.7	21.7	23.7(7)	10(2)	26(1)	62(2)
400	26.3	7.4	35.2	28(2)	7(4)	31(2)	69(5)
450	28.5	6.2	37.6	30(2)	6(5)	34(3)	72(6)

https://doi.org/10.1180/minmag.2017.081.037 Published online by Cambridge University Press

and non-linear optical properties are planned for the near future.

Acknowledgements

We are grateful to Edward Grew, Peter Leverett, Anna Garavelli and an anonymous reviewer for valuable comments. This work was supported financially by the Russian Science Foundation through the grant 16-17-10085. Technical support by the SPbSU X-ray Diffraction and Microscopy and Microanalysis Resource Centres are gratefully acknowledged.

Supplementary material

To view supplementary material for this article, please visit https://doi.org/10.1180/minmag.2017.081.037

References

Balić-Žunić, T., Garavelli, A., Acquafredda, P., Leonardsen, E. and Jakobsson, S.P. (2009) Eldfellite, $NaFe(SO_4)_2$, a new fumarolic mineral from Eldfell volcano, Iceland. *Mineralogical Magazine*, **73**, 51–57.

Barpanda, P., Oyama, G., Ling, C.D. and Yamada, A. (2014) Kröhnkite-type $Na_2Fe(SO_4)_2{\cdot}2H_2O$ as a novel 3.25 v insertion compound for Na-ion batteries. *Chemistry of Materials*, **26**, 1297–1299.

Behera, J.N. and Rao, C.N.R. (2006) Amine-templated one-dimensional metal sulfates including a mixed-valent Fe compound with a half-kagome structure. *Chemistry – An Asian Journal*, **1**, 742–750.

Brese, N.E. and O'Keeffe, M. (1991) Bond-valence parameters for solids. *Acta Crystallographica*, **B47**, 192–197.

Burns, P.C. and Hawthorne, F.C. (1995) Coordination geometry pathways in Cu^{2+} oxysalt minerals. *Canadian Mineralogist*, **33**, 889–905.

Chevrier, G., Giester, G. and Zemann, J. (1993) Neutron refinements of $NaCu_2(H_3O_2)(SO_4)_2$ and $RbCu_2(H_3O_2)(SeO_4)_2$: variation of the hydrogen bond system in the natrochalcite-type series. *Zeitschrift für Kristallographie – Crystalline Materials*, **206**, 7–14.

Dahlman, B. (1952) The crystal structures of kröhnkite, and brandtite. *Arkiv för Mineralogi och Geologi*, **1**, 339–366.

Demartin, F., Campostrini, I., Castellano, C., Gramaccioli, C.M. and Russo, M. (2012) D'ansite-(Mn), $Na_{21}Mn^{2+}(SO_4)_{10}Cl_3$ and d'ansite-(Fe), $Na_{21}Fe^{2+}(SO_4)_{10}Cl_3$, two new minerals from volcanic fumaroles. *Mineralogical Magazine*, **76**, 2773–2783.

Domeyko, I. (1879) Kronnkit. Pp. 250–252 in: *Mineralojía*. Libreria Central de Servat I CA, Santiago, Chile.

Driscoll, L.L., Kendrick, E., Wright, A.J. and Slater, P.R. (2016) Investigation into the effect on structure of oxoanion doping in $Na_2M(SO_4)_2{\cdot}2H_2O$. *Journal of Solid State Chemistry*, **242**, 103–111.

Firsova, V.A., Bubnova, R.S. and Filatov, S.K. (2011) *Program for the Thermal Expansion Tensor Determination for Crystalline Materials*. Institute of Silicate Chemistry of Russian Academy of Science, St. Petersburg, Russia.

Fleck, M. and Kolitsch, U. (2003) Natural and synthetic compounds with kröhnkite-type chains. An update. *Zeitschrift für Kristallographie – Crystalline Materials*, **218**, 553–567.

Fleck, M., Kolitsch, U., Hertweck, B., Giester, G., Wildner, M., Prem, M. and Wohlschläger, A. (2002*a*) Crystal structures of the double salt dihydrates $K_2Cd(SeO_4)_2{\cdot}2H_2O$, $K_2Mn(SO_4)_2{\cdot}2H_2O$, $(NH_4)_2Cu(SeO_4)_2{\cdot}2H_2O$ and $KFeH(SO_4)_2{\cdot}2H_2O$. *Zeitschrift für Kristallographie – Crystalline Materials*, **217**, 242–248.

Fleck, M., Kolitsch, U. and Hertweck, B. (2002*b*) Natural and synthetic compounds with kröhnkite-type chains: Review and classification. *Zeitschrift für Kristallographie – Crystalline Materials*, **217**, 435–443.

Hawthorne, F.C. and Ferguson, R.B. (1975) Refinement of the crystal structure of kroehnkite. *Acta Crystallographica*, **B31**, 1753–1755.

Hawthorne, F.C., Krivovichev, S.V. and Burns, P.C. (2000) The crystal chemistry of sulfate minerals. Pp. 1–112 in: *Sulfate Minerals – Crystallography, Geochemistry and Environmental Significance* (C.N. Alpers, J.L. Jambor, D.K. Nordstrom, editors). Reviews in Mineralogy & Geochemistry, **vol. 40**. Mineralogical Society of America and the Geochemical Society, Chantilly, Virginia, USA.

Kolitsch, U. and Fleck, M. (2005) Second update on compounds with kröhnkite-type chains. *Zeitschrift für Kristallographie – Crystalline Materials*, **220**, 31–41.

Kolitsch, U. and Fleck, M. (2006) Third update on compounds with kröhnkite-type chains: The crystal structure of wendwilsonite $[Ca_2Mg(AsO_4)_2{\cdot}2H_2O]$ and the new triclinic structure types of synthetic $AgSc(CrO_4)_2{\cdot}2H_2O$ and $M_2Cu(Cr_2O_7)_2{\cdot}2H_2O$ (M = Rb, Cs). *European Journal of Mineralogy*, **18**, 471–482.

Leftwich, K., Bish, D.L. and Chen, C.H. (2012) Crystal structure and hydration/dehydration behavior of $Na_2Mg(SO_4)_2{\cdot}16H_2O$: A new hydrate phase observed under Mars-relevant conditions. *American Mineralogist*, **98**, 1772–1778.

Majzlan, J., Zittlau, A.H., Grevel, K.-D., Schliesser, J., Woodfield, B.F., Dachs, E., Števko, M., Chovan, M., Plášil, J., Sejkora, J. and Milovská, S. (2016) Thermodynamic properties and phase equilibria of

the secondary copper minerals libethenite, olivenite, pseudomalachite, kröhnkite, cyanochroite, and devilline. *Canadian Mineralogist*, **53**, 937–960.

Mandarino, J.A. (1981) The Gladstone-Dale relationship: Part IV. The compatibility concept and its application. *Canadian Mineralogist*, **19**, 441–450.

Marinova, D., Kostov, V., Nikolova, R., Kukeva, R., Zhecheva, E., Sendova-Vasileva, M. and Stoyanova, R. (2015) From kröhnkite- to alluaudite-type of structure: Novel method of synthesis of sodium manganese sulfates with electrochemical properties in alkali-metal ion batteries. *Journal of Materials Chemistry*, **A3**, 22287–22299.

Mills, S.J., Wilson, S.A., Dipple, G.M. and Raudsepp, M. (2010) The decomposition of konyaite: Importance in CO_2 fixation in mine tailings. *Mineralogical Magazine*, **74**, 903–917.

Mills, S.J., Nestola, F., Kahlenberg, V., Christy, A.G., Hejny, C. and Redhammer, G.J. (2013) Looking for jarosite on Mars: the low-temperature crystal structure of jarosite. *American Mineralogist*, **98**, 1966–1971.

Nadeem, M.A., Bhadbhade, M., Bircher, R. and Stride, J. A. (2010) Three isolated structural motifs in one crystal: penetration of two 1D chains through large cavities within 2D polymeric sheets. *CrystEngComm*, **12**, 1391–1393.

Nazarchuk, E.V., Siidra, O.I., Agakhanov, A.A., Lukina, E.A., Avdontseva, E.Y. and Karpov, G.A. (2018) Itelmenite, $Na_2CuMg_2(SO_4)_4$, a new anhydrous sulphate mineral from the Tolbachik volcano. *Mineralogical Magazine*, in press https://doi.org/10.1180/minmag.2017.081.089

Pasha, I., Choudhury, A. and Rao, C.N.R. (2003) The first organically templated linear metal selenite. *Journal of Solid State Chemistry*, **174**, 386–391.

Peterson, R.C. and Wang, R. (2006) Crystal molds on Mars: Melting of a possible new mineral species to create Martian chaotic terrain. *Geology*, **34**, 957–960.

Saha, D., Madras, G. and Guru Row, T.N. (2011) Manipulation of the hydration levels in minerals of sodium cadmium bisulfate toward the design of functional materials. *Crystal Growth and Design*, **11**, 3213–3221.

Sheldrick, G.M. (2015) New features added to the refinement program SHELXL since 2008 are described and explained. *Acta Crystallographica*, **C71**, 3–8.

Siidra, O.I., Vergasova, L.P., Kretser, Y.L., Polekhovsky, Y.S., Filatov, S.K. and Krivovichev, S. V. (2014) Unique thallium mineralization in the fumaroles of the Tolbachik volcano, Kamchatka Peninsula, Russia. II. Karpovite, $Tl_2VO(SO_4)_2(H_2O)$. *Mineralogical Magazine*, **78**, 1699–1709.

Siidra, O.I., Nazarchuk, E.V., Agakhanov, A.A., Lukina, E.A., Zaitsev, A.N., Turner, R., Filatov, S. K., Pekov, I.V., Karpov, G.A. and Yapaskurt, V.O. (2018) Hermannjahnite, $CuZn(SO_4)_2$, a new mineral with chalcocyanite derivative structure from the Naboko scoria cone of the 2012–2013 fissure eruption at Tolbachik volcano, Kamchatka, Russia. *Mineralogy and Petrology*, **112**, 123–134.

Siidra, O.I., Nazarchuk, E.V., Zaitsev, A.N., Lukina, E.A., Avdontseva, E.Y., Vergasova, L.P., Vlasenko, N.S., Filatov, S.K., Turner, R. and Karpov, G.A. (2017) Copper oxosulphates from fumaroles of Tolbachik vulcano: puninite, $Na_2Cu_3O(SO_4)_3$ – a new mineral species and structure refinements of kamchatkite and alumoklyuchevskite. *European Journal of Mineralogy*, **29**, 499–510.

Stoilova, D., Marinova, D., Wildner, M. and Georgiev, M. (2009*a*) Comparative study on energetic distortions of SO_4^{2-} ions matrix-isolated in compounds with kröhnkite-type chains, $K_2Me(CrO_4)_2{\cdot}2H_2O$ and $Na_2Me(SeO_4)_2{\cdot}2H_2O$ (Me = Mg, Co, Ni, Zn, Cd). *Solid State Sciences*, **11**, 2044–2050.

Stoilova, D., Marinova, D. and Georgiev, M. (2009*b*) Hydrogen bond strength in chromates with kröhnkite-type chains, $K_2Me(CrO_4)_2{\cdot}2H_2O$ (Me = Mg, Co, Ni, Zn, Cd). *Vibrational Spectroscopy*, **50**, 245–249.

Szynkiewicz, A., Borrok, D.M. and Vaniman, D.T. (2014) Efflorescence as a source of hydrated sulfate minerals in valley settings on Mars. *Earth and Planetary Science Letters*, **393**, 14–25.

Testasicca, L.P., Frost, R.L., Ruan, X., Lima, J., Belotti, F. M. and Scholz, R. (2016) The application of high-temperature X-ray diffraction and infrared emission spectroscopy to the thermal decomposition of kröhnkite. *Journal of Thermal Analysis and Calorimetry*, **126**, 1089–1095.

Vaniman, D.T., Bish, D.L., Chipera, S.J., Fialips, C.I., Carey, J.W. and Feldman, W.G. (2004) Magnesium sulphate salts and the history of water on Mars. *Nature*, **431**, 663–665.

Vasavada, A. (2017) Our changing view of Mars. *Physics Today*, **70**, 34–41.

Vergasova, L.P. and Filatov, S.K. (2016) A study of volcanogenic exhalation mineralization. *Journal of Volcanology and Seismology*, **10**, 71–85.

Wang, A and Zhou, A. (2014) Experimental comparison of the pathways and rates of the dehydration of Al-, Fe-, Mg- and Ca-sulfates under Mars relevant conditions. *Icarus*, **234**, 162–173.

Wierzbicka-Wieczorek, M., Kolitsch, U. and Tillmanns, E. (2008) Flux syntheses and crystal structures of new compounds with decorated kröhnkite-like chains. *Acta Chimica Slovenica*, **55**, 909–917.

Wildner, M. and Stoilova, D. (2003) Crystal structures and crystal chemical relationships of kröhnkite- and collinsite-type compounds $Na_2Me^{2+}(XO_4)_2{\cdot}2H_2O$ (X = S, Me = Mn, Cd; and X = Se, Me = Mn, Co, Ni, Zn, Cd) and $K_2Co(SeO_4)_2{\cdot}2H_2O$. *Zeitschrift für Kristallographie – Crystalline Materials*, **218**, 201–209.

https://doi.org/10.1180/minmag.2017.081.037 Published online by Cambridge University Press

Yang, H., Jenkins, R.A., Downs, R.T., Evans, S.H. and Tait, K.T. (2011) Rruffite, $Ca_2Cu(AsO_4)_2 \cdot 2H_2O$, a new member of the roselite group, from Tierra Amarilla, Chile. *Canadian Mineralogist*, **49**, 877–884.

Yoshiasa, A., Yagyu, G., Ito, T., Yamanaka, T. and Nagai, T. (2000) Crystal structure of the high pressure phase(II) in $CuGeO_3$. *Zeitschrift für Anorganische und Allgemeine Chemie*, **626**, 36–41.

https://doi.org/10.1180/minmag.2017.081.037 Published online by Cambridge University Press